**MATERIALS SCIENCE / МАТЕРИАЛОВЕДЕНИЕ**

**UDC** 669.046:533.9
**DOI** 10.17073/0368-0797-2025-3-266-273



***Original article***
***Оригинальная статья***

# PECULIARITIES OF DEFORMATION LOCALIZATION IN ADDITIVE MATERIAL WITH STRUCTURAL-PHASE HETEROGENEITY

**D. V. Orlova, G. V. Shlyakhova, M. V. Nadezhkin**

**Institute of Strength Physics and Materials Science, Siberian Branch of the Russian Academy of Sciences** (2/4 Akademicheskii Ave., Tomsk 634055, Russian Federation)

dvo@ispms.ru

***Abstract***. Creation of compounds of dissimilar metals is one of the priority areas in the field of obtaining special structural materials with a unique combination of properties. In connection with development of new production processes, the question arises about the influence of structural-phase heterogeneity of multilayer materials on deformation behavior. In particular, an important scientific problem is the localization of plastic flow. The digital image correlation (DIC) method was used to analyze the nature of localized plastic deformation in the bimetallic composite austenitic stainless steel/low-carbon steel manufactured by additive beam technology. It was found that in all layers of the bimetal, plastic deformation develops locally in each layer of the studied composite according to the loading stages. It is shown that during deformation of a bimetallic compound, the appearance of the yield plateau stage ($n = 0$) and, accordingly, the Lüders deformation is suppressed, despite the significant content of a low-carbon steel layer in the bimetal. In the parabolic section with the hardening index $n = 0.5$, the components of local elongations $\varepsilon_{xx}$ form a stationary periodic distribution of localized deformation zones. With the onset of the stage with $n \leq 0.5$, a high-amplitude deformation zone is observed in the transition layer, which coincides with the place of future sample fracture. In this case, the growth of the amplitude of localized deformation in this zone begins at the parabolic stage of the loading diagram. Structural heterogeneity at the interface in the bimetallic composite austenitic stainless steel/low-carbon steel is the source of the initiation of a fracture crack in the austenitic steel layer. Apparently, the initiation of the destruction zone in the transition layer is associated with the formation of a brittle carburized layer, which occurs due to the diffusion of carbon through the interface low-carbon steel – stainless steel.

***Keywords:*** bimetal, austenitic stainless steel, carbon steel, microstructure, phase composition, localized deformation, DIC

***Acknowledgements:*** The work was supported by the Russian Science Foundation, grant No. 24-29-00580 https://rscf.ru/project/24-29-00580/. The authors express their gratitude to the staff of the Laboratory for Quality Control of Materials and Structures of the Institute of Strength Physics and Materials Science SB RAS for their assistance in manufacturing the bimetallic compound.

***For citation:*** Orlova D.V., Shlyakhova G.V., Nadezhkin M.V. Peculiarities of deformation localization in additive material with structural-phase heterogeneity. *Izvestiya. Ferrous Metallurgy*. 2025;68(3):266–273. *https://doi.org/10.17073/0368-0797-2025-3-266-273*

# ОСОБЕННОСТИ ЛОКАЛИЗАЦИИ ДЕФОРМАЦИИ В АДДИТИВНОМ МАТЕРИАЛЕ СО СТРУКТУРНО-ФАЗОВОЙ НЕОДНОРОДНОСТЬЮ

**Д. В. Орлова, Г. В. Шляхова, М. В. Надежкин**

**Институт физики прочности и материаловедения Сибирского отделения РАН** (Россия, 634055, Томск, пр. Академический, 2/4)

dvo@ispms.ru

***Аннотация***. Создание соединений разнородных металлов является одним из приоритетных направлений в области получения специальных конструкционных материалов с уникальным сочетанием свойств. В связи с развитием новых производственных процессов встает вопрос о влиянии структурно-фазовой неоднородности многослойных материалов на деформационное поведение. В частности, важной научной проблемой является локализация пластического течения. В настоящей работе для анализа характера локализованной пластической деформации в биметаллическом соединении аустенитная нержавеющая сталь – низкоуглеродистая сталь, изготовленном аддитивной лучевой технологией, использовался метод цифровой корреляции изображений (DIC). Во всех слоях биметалла пластическая деформация развивается локализованно в соответствии со стадийностью кривой нагружения. При дефор-

 

мировании биметаллического соединения подавляется появление стадии площадки текучести ($n = 0$) и, соответственно, деформации Людерса, несмотря на значительное содержание в биметалле слоя низкоуглеродистой стали. На параболическом участке с показателем упрочнения $n = 0,5$ компоненты локальных удлинений $\varepsilon_{xx}$ формируют стационарное периодическое распределение зон локализованной деформации. С наступлением стадии с $n \leq 0,5$ наблюдается высокоамплитудная зона деформации в переходном слое, которая совпадает с местом будущего разрушения образца. При этом рост амплитуды локализованной деформации в этой зоне начинается еще на параболической стадии диаграммы нагружения. Структурная неоднородность у границы раздела в биметаллическом соединении аустенитная нержавеющая сталь – низкоуглеродистая сталь является источником зарождения разрушающей трещины в слое аустенитной стали. По-видимому, зарождение зоны разрушения в переходном слое связано с формированием хрупкого науглероженного слоя, происходящим из-за диффузии углерода через границу раздела низкоуглеродистая сталь – нержавеющая сталь.

***Ключевые слова:*** биметалл, аустенитная нержавеющая сталь, углеродистая сталь, микроструктура, фазовый состав, локальная деформация, DIC

***Благодарности:*** Работа выполнена при финансовой поддержке гранта РНФ, тема № 24-29-00580 https://rscf.ru/project/24-29-00580/. Авторы выражают благодарность сотрудникам лаборатории контроля качества материалов и конструкций Института физики прочности и материаловедения Сибирского отделения РАН за помощь в изготовлении биметаллического соединения.

***Для цитирования:*** Орлова Д.В., Шляхова Г.В., Надежкин М.В. Особенности локализации деформации в аддитивном материале со структурно-фазовой неоднородностью. *Известия вузов. Черная металлургия*. 2025;68(3):266–273.
https://doi.org/10.17073/0368-0797-2025-3-266-273

## Introduction

At present, increasing attention is being paid to the development of two-layer metallic composites consisting of a carbon steel base coated with a protective layer of stainless steel. These materials combine the good weldability, formability, and thermal conductivity of carbon steel with the high corrosion and wear resistance of stainless steel [1 – 4]. A particularly promising approach in this regard is additive electron beam cladding, which involves the layer-by-layer deposition of material by melting solid or powder metal wires [2; 5 – 7]. Control over processing parameters and the composition of alloying elements makes it possible to produce metal layers with the desired physical, mechanical, and geometrical characteristics. Most current research on such composites focuses on issues such as residual stresses, microstructural anisotropy, and pore formation [5]. However, multilayer composites produced in this way are subsequently subjected to processes such as cutting, forging, rolling, bending, and joining. This raises important questions about the influence of structural-phase heterogeneity on the deformation behavior of these materials.

At the same time, previous studies have shown that even single crystals and structurally homogeneous materials tend to develop zones under loading where localized deformation significantly exceeds the average strain [8; 9]. Macroscopic localization of plastic deformation exhibits autowave behavior and, depending on the stage of plastic flow, may manifest as a switching autowave (as in the case of Chernov–Lüders bands), a stationary dissipative structure during the parabolic strain hardening stage, or an autowave collapse in the stage preceding fracture. Consequently, a clear understanding of the kinetics of localized plastic deformation is critical for advancing technologies related to the manufacturing and application of bimetallic composites.

The digital image correlation (DIC) method, in combination with mechanical testing, has proven effective for analyzing the stress – strain state of both cast [10; 11] and additively manufactured materials [12 – 14]. However, the most existing studies on deformation in additively produced materials are conducted on samples of various orientations cut from billets, without considering the influence of the substrate interface.

Given that combining dissimilar metals into a single bimetallic structure inevitably introduces macroscopic heterogeneity in both structure and mechanical properties, it is essential to investigate how localized plastic flow evolves under mechanical loading in such systems.

The aim of the present study is to investigate the characteristics of macrolocalization of plastic deformation during tensile loading of an austenitic stainless steel – low-carbon steel composite fabricated by additive electron beam cladding.

## Materials and methods

The bimetallic composite was produced by electron beam cladding in a vacuum chamber through multiple passes of AISI 308L austenitic stainless steel wire (wt. %: <0.4 C; 9 – 12 Ni; 18 – 21 Cr) onto a low-carbon steel substrate (wt. %: 0.14 – 0.22 C; 0.12 – 0.30 Si; 0.40 – 0.65 Mn) with a thickness of 4 mm. The welding wire had a diameter of 1.2 mm. The cladding process was carried out at an accelerating voltage of 30 kV and a beam current of 70 mA, with a wire feed rate of $3 \cdot 10^{-3}$ m/s. Test samples were prepared by electrical discharge machining (EDM) in the form of double-sided flat dog-bone samples. Each sample had a gauge length of 40 mm, width of 10 mm, and thickness of 2 mm, with the interface between the two metals positioned along the centerline. Uniaxial tensile testing was conducted at room temperature using a Walter + Bai AG LFM 125 universal testing

machine. The crosshead speed was set at 0.2 mm/min, corresponding to a strain rate of $8.33 \cdot 10^{-5}$ $s^{-1}$.

To detect zones of localized deformation, a sequence of digital images of the deforming sample was recorded. A speckle pattern was generated by illuminating the sample with coherent light from a semiconductor laser (wavelength 635 nm, power 15 mW). The images were captured using a Point Grey FL3-GE-50S5MC digital camera with a resolution of 2448×2048 px at a frame rate of 5 frames per second. The camera was positioned 0.3 m from the sample, providing a spatial resolution of 20.4 μm/px. Post-processing of the image sequences was performed using the digital image correlation (DIC) method [10; 11], which enables precise measurement of displacement fields, strain components, and strain rate distributions.

Microstructural characterization was carried out using optical microscopy with standard metallographic preparation techniques, as well as atomic force microscopy (AFM) in Phase mode, using a Solver PRO–47H system (NT-MDT, Zelenogorsk, Russia). Fractographic analysis of the fracture surfaces was performed using a LEO EVO 50 scanning electron microscope (Zeiss, Germany).

## Results and discussion

### *Microstructure and mechanical properties*

The typical microstructure of the clad layers formed by vacuum electron beam additive melting of austenitic steel is biphasic (FCC + BCC), consisting of γ-austenite dendrites interspersed with thin δ-ferrite interlayers (Fig. 1, *a*, *b*). A finely dispersed acicular structure approximately 1.3 mm thick forms near the fusion boundary (Fig. 1, *a*), corresponding to regions of elevated microhardness (Fig. 1, *c*). The remaining clad region also exhibits a dendritic structure (Fig. 1, *b*), but is characterized by lower microhardness values (Fig. 1, *c*), which is likely due to dendrite coarsening and a reduction in δ-ferrite content, as confirmed by AFM images (Fig. 1, *d*, *e*). The microstructure of the substrate material consists of ferrite grains with an average size of 60 ± 15 μm and pearlite. On the carbon steel side of the fusion boundary, a decarburized zone approximately 250 μm thick is observed.

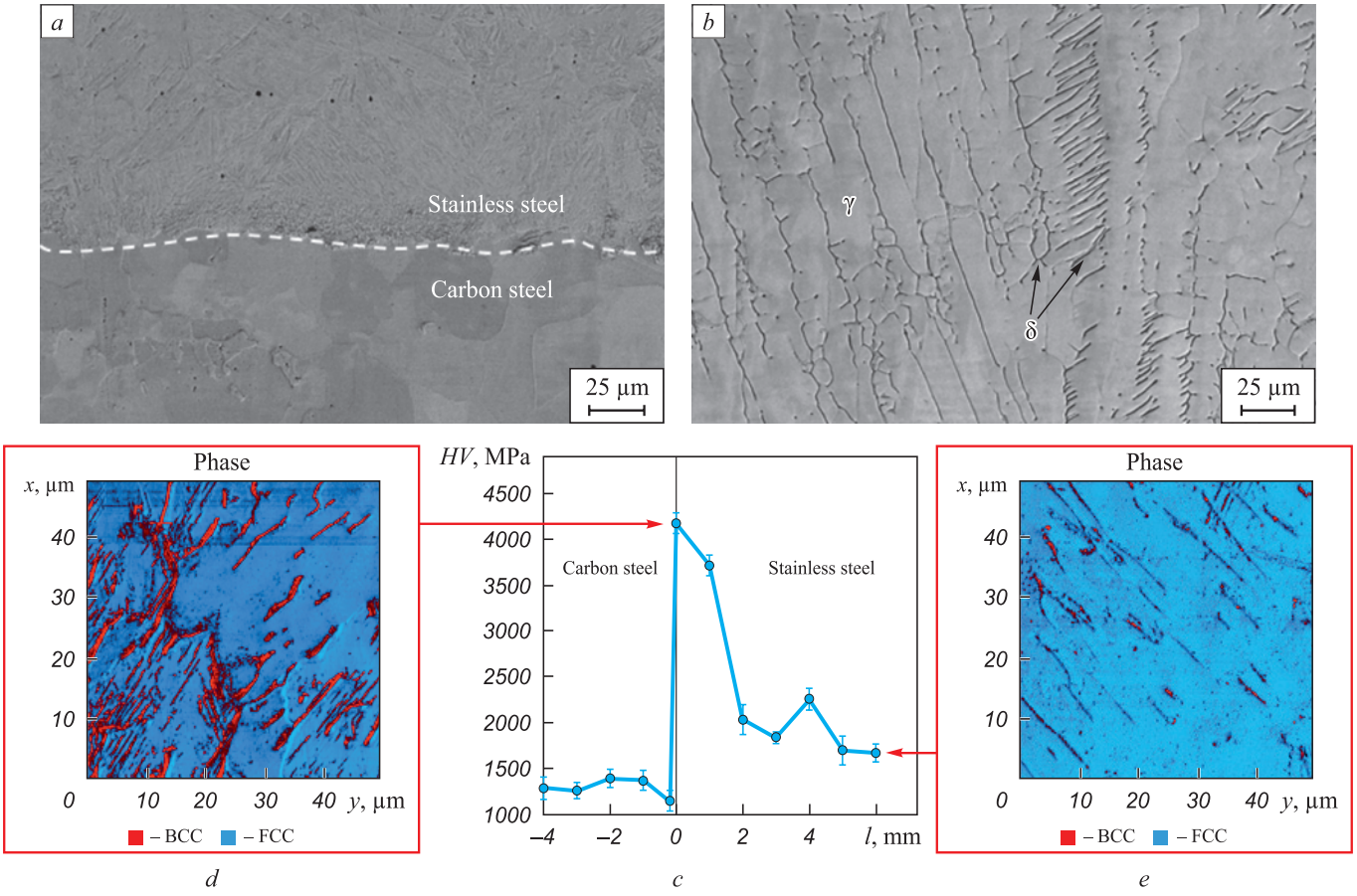


***Fig. 1.*** Microstructure of bimetallic composite (*a*, *b*), distribution of microhardness across the sample width (*c*), arrows show AFM images of the structure in the "Phase" mode (*d*, *e*)

***Рис. 1.*** Микроструктура биметаллического соединения (*a*, *b*), распределение микротвердости по ширине рабочей части образца (*c*), стрелками показаны АСМ изображения структуры в режиме «Фаза» (*d*, *e*)

Fig. 2 and the accompanying Table present the engineering loading diagrams (σ–ε) for the bimetallic samples and the corresponding cast metals, along with their principal mechanical properties. According to tensile testing, the engineering loading diagrams of the additively manufactured bimetal correspond to a general type typically described by a parabolic function of the form $\sigma = \sigma_0 + K\sigma^n$ (where $K$ is the strain hardening coefficient; $n \leq 1.0$ is the hardening index). Based on the value of $n$, four characteristic stages can be distinguished: the yield plateau ($n = 0$), linear strain hardening ($n = 1.0$), parabolic strain hardening ($n = 0.5$), and pre-fracture ($n \leq 0.5$). In the case of the bimetallic samples studied, only two stages are observed: the parabolic strain hardening stage ($n = 0.5$) and the pre-fracture stage ($n \leq 0.5$). The strain intervals corresponding to each stage (Δε) are provided in the table. Despite the elevated hardness observed in the interfacial region – which is atypical for both the stainless steel and the carbon steel substrate – the bimetallic sample exhibits high ductility.

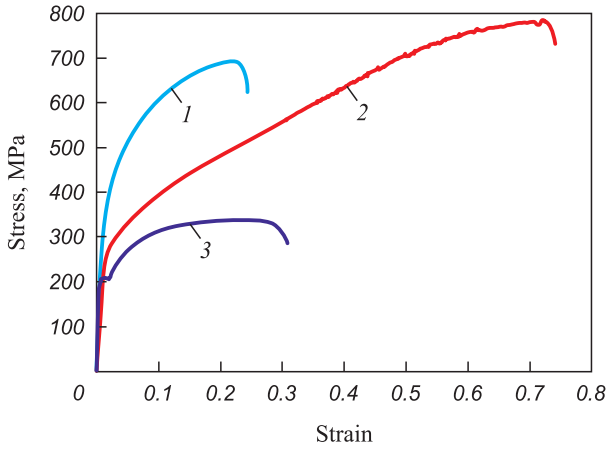


***Fig. 2.*** Engineering stress – engineering strain curves for bimetal composite (*1*) and cast metals:
*2* – austenitic stainless steel;
*3* – low carbon steel

***Рис. 2.*** Кривые нагружения в координатах условное напряжение – условная деформация биметалла (*1*) и литых металлов:
*2* – аустенитная нержавеющая сталь;
*3* – низкоуглеродистая сталь

## Distribution of localized deformation

According to the autowave theory of plasticity, the strain hardening stage corresponds to a specific autowave mode of localized plasticity [8; 9; 15]. For instance, during the yield plateau – characteristic of low-carbon steels and certain other alloys – a propagating front of localized deformation is observed along the tensile axis of the sample. This front represents a switching autowave that transitions the material from a metastable (elastic) to a stable (plastic) state [16 – 19]. In homogeneous metallic materials, the parabolic strain hardening stage corresponds to a spatially periodic distribution of localization sites, forming a stationary dissipative structure. The stage preceding fracture is associated with autowave collapse [9].

It was demonstrated in [20] that during tensile testing of a three-layer composite consisting of a carbon steel core and two stainless steel cladding layers, the loading diagram retains a yield plateau. Analysis of the strain localization patterns revealed that the Lüders band in the carbon steel core was bounded by two fronts propagating in opposite directions along the bimetal's tensile axis at different velocities. Thus, although the presence of thin stainless steel cladding layers shortened the duration of the yield plateau, it did not fully suppress the manifestation of Lüders deformation in the bimetal.

In the present study, the engineering loading diagrams of the additively manufactured bimetal do not exhibit a yield plateau, despite the substantial content of low-carbon steel in the material (see Table). Consequently, no switching autowave in the form of a propagating Chernov–Lüders band is observed.

Fig. 3, *a*, *c* shows the cumulative distribution of local elongation $\varepsilon_{xx}(x)$ within the parabolic strain hardening stage ($n = 0.5$) across the three layers of the investigated bimetal. During this stage, each of the identified layers exhibits a stationary, periodic distribution of localized deformation zones (stationary dissipative structures) with a spatial period λ, similar to those found in homogeneous samples [9]. In the subsequent pre-fracture

**Mechanical characteristics of materials and total strain intervals Δε for plastic flow stages**

**Механические характеристики материалов и продолжительность Δε стадий пластического течения**

| Metal | | Yield strength, MPa | Ultimate strength, MPa | Elongation | Δε for plastic flow stages | | | |
|---|---|---|---|---|---|---|---|---|
| | | | | | $n = 0$ | $n = 1.0$ | $n = 0.5$ | $n \leq 0.5$ |
| Cast materials | Carbon steel | 209 ± 4.5 | 339 ± 4.5 | 0.30 ± 0.05 | 0.008 – 0.022 | – | 0.028 – 0.057 | 0.07 – 0.28 |
| | Stainless steel | 262 ± 3.0 | 780 ± 5.0 | 0.70 ± 0.10 | – | 0.05 – 0.32 | – | 0.32 – 0.69 |
| Bimetal | | 330 ± 5.0 | 693 ± 5.0 | 0.25 ± 0.05 | – | – | 0.022 – 0.170 | 0.17 – 0.22 |

stage ($n \leq 0.5$), a significant increase in the amplitude of $\varepsilon_{xx}$ occurs in one of the localized deformation zones (Fig. 3, *a*, *b*), which, within the autowave framework, corresponds to autowave collapse.

To analyze the rate of localized strain accumulation, seven regions measuring 1.5 mm$^2$ each were selected along the fusion boundary at 5 mm intervals, ranging from $x_1 = 1$ mm to $x_7 = 36$ mm along the gauge length. The accumulation rates of localized deformation $\varepsilon_{xx}$ in these regions are presented in Fig. 3, *d*. The slope of each curve reveals that strain accumulates at different rates across regions *1* through *7*. Initially, deformation proceeds most intensively in region *1*. However, at $t^* = 1860$ s ($\varepsilon = 15.5$ %) a sudden increase in the strain accumulation rate is recorded in region *7*, rising from $0.68 \cdot 10^{-4}$ to $8.37 \cdot 10^{-4}$ s$^{-1}$. This region ($x_7 = 36$ mm) corresponds to the actual fracture initiation site. A drop on the loading diagram, indicating the onset of instability, and the appearance of a visible neck were observed at $t = 2640$ s ($\varepsilon = 22$ %).

As shown in Fig. 3, *d*, at this point strain accumulation ceases in all other regions, while continuing only in region *7*, where the distractive crack initiates. Thus, the strain distribution patterns allow the crack initiation site to be identified as early as 30 % before structural instability and 8 % before the onset of the pre-fracture stage.

Fracture in the bimetallic composite samples occurs through crack propagation from the interface into

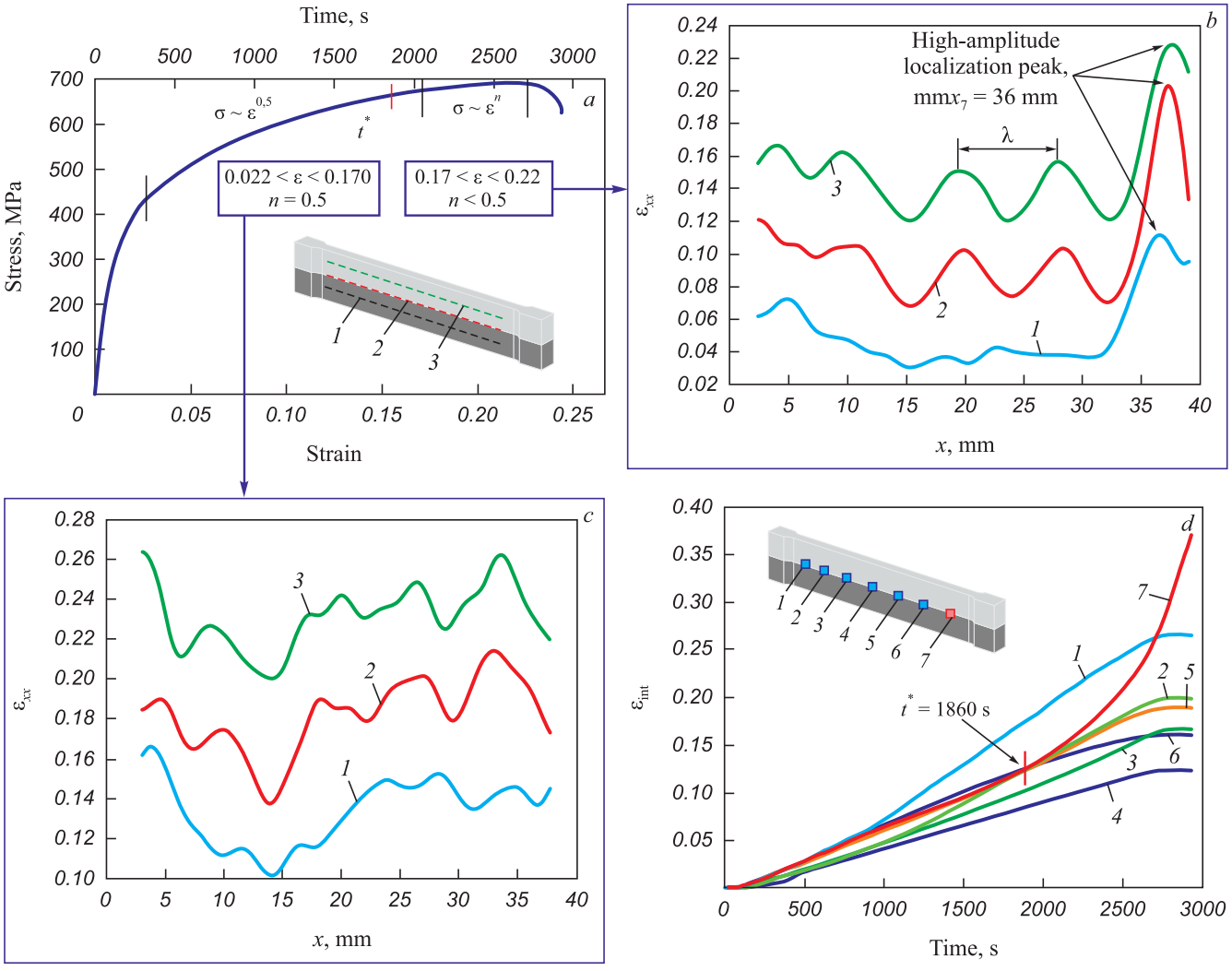


***Fig. 3.*** Total distribution of local elongations $\varepsilon_{xx}(x)$ in the layers of bimetallic compound (*a* – *c*) and rate of deformation accumulation on bimetal fusion line at points *1* – *7* (*d*:
*1* – carbon steel; *2* – fusion boundary; *3* – deposited metal at parabolic (*a*, *c*) and pre–fracture stages (*a*, *b*)
(for clarity, $\varepsilon_{xx}(x)$ in layers *2* and *3* is shifted relative to layer *1* along the *y* axis by 0.05 and 0.10, respectively)

***Рис. 3.*** Суммарное распределение локальных удлинений $\varepsilon_{xx}(x)$ в слоях биметаллического соединения (*a* – *c*) и скорость накопления деформации на линии сплавления биметалла в точках *1* – *7* (*d*):
*1* – углеродистая сталь; *2* – граница сплавления; *3* – наплавленный металл на параболической (*a*, *c*) и стадии предразрушения (*a*, *b*)
(для наглядности $\varepsilon_{xx}$ в слоях *2* и *3* смещена относительно слоя *1* по оси *y* на 0,05 и 0,10 соответственно)

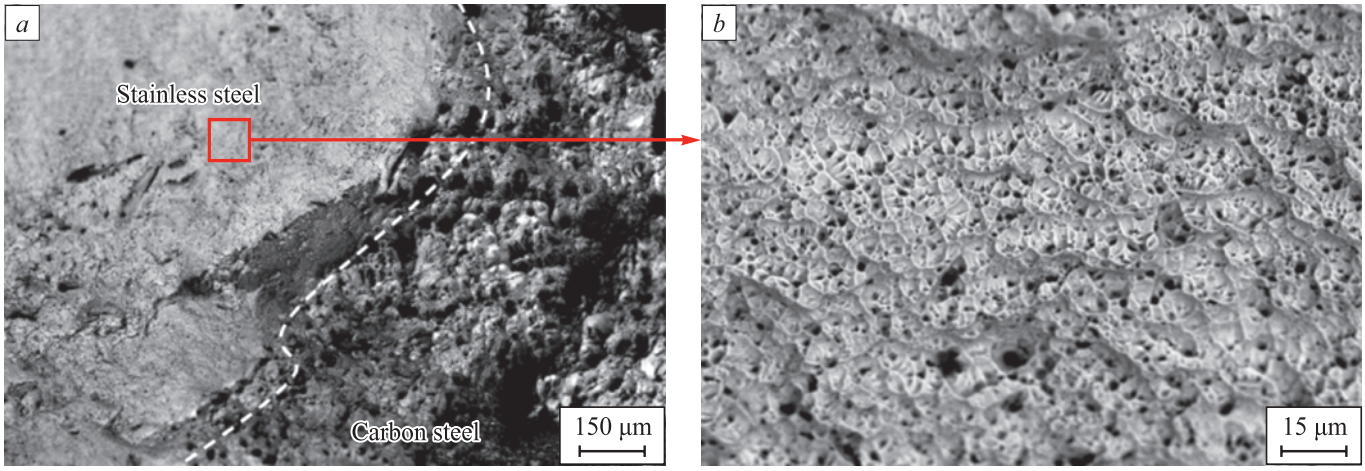


***Fig. 4.*** Fractography of bimetallic compound sample after stretching

***Рис. 4.*** Фрактография образца биметаллического соединения после растяжения

the clad layer. The origin of the fracture zone in the transition region is presumably associated with the formation of a brittle carburized layer, caused by carbon diffusion from the substrate metal into the deposited metal (Fig. 1). Fig. 4 presents the fracture surface morphology after stretching (tensile testing). Numerous dimples and micropores are visible on the fracture surface of the austenitic stainless steel layer, indicating a typical dimple rupture mechanism characteristic of ductile failure. Most of the dimples range in size from 5 to 15 μm. In the carbon steel layer, smooth and shiny areas are present, suggesting a mixed ductile–brittle fracture mode. No delamination was observed along the fusion boundary between the dissimilar metals.

## Conclusions

The study demonstrated that localized plastic deformation occurs throughout the loading process in each layer of the bimetallic composite consisting of austenitic stainless steel and low-carbon steel, fabricated by electron beam additive cladding. The engineering loading diagram of the bimetal shows only two distinct stages – parabolic hardening and pre-fracture – while the yield plateau is suppressed.

Initially, during the parabolic hardening stage (hardening index $n = 0.5$), a stationary distribution of localized plasticity zones is formed. As the material enters the stage with $n \leq 0.5$, a high-amplitude deformation zone emerges within the transition layer, coinciding with the future fracture location. Notably, the amplitude growth of localized deformation begins even during the parabolic hardening stage. The structural heterogeneity introduced by the interface between low-carbon and austenitic steels in the bimetallic composite serves as the origin of crack initiation, which propagates into the austenitic steel layer.

## References / Список литературы

1. Li Zh., Zhao J., Jia F., Zhang Q., Liang X., Jiao S., Jiang Zh. Numerical and experimental investigation on the forming behaviour of stainless/carbon steel bimetal composite. *Journal of Advanced Manufacturing Technology*. 2019; 101:1075–1083. https://doi.org/10.1007/s00170-018-2985-7
2. Shen W., Feng L., Feng H., Cao Y., Liu L., Cao M., Ge Y. Preparation and characterization of 304 stainless steel/ Q235 carbon steel composite material. *Results in Physics*. 2017;7:529–534. https://doi.org/10.1016/j.rinp.2016.12.050
3. Li H., Zhang L., Zhang B., Zhang Q. Interfacial fracture behavior of a stainless/carbon steel bimetal plate in a uniaxial tension test. *Results in Physics*. 2019;14:102470. https://doi.org/10.1016/j.rinp.2019.102470
4. Dhib Z., Guermazi N., Gaspérini M., Haddar N. Cladding of low-carbon steel to austenitic stainless steel by hot-roll bonding: microstructure and mechanical properties before and after welding. *Materials Science and Engineering: A*. 2016;656:130–141. https://doi.org/10.1016/j.msea.2015.12.088
5. Bajaj P., Hariharan A., Kini A., Kürnsteiner P., Raabe D., Jägle E.A. Steels in additive manufacturing: A review of their microstructure and properties. *Materials Science and Engineering: A*. 2020;772:138633. https://doi.org/10.1016/j.msea.2019.138633
6. Tarasov S.Yu., Filippov A.V., Shamarin N.N., Fortuna S.V., Maier G.G., Kolubaev E.A. Microstructural evolution and chemical corrosion of electron beam wire-feed additively manufactured AISI 304 stainless steel. *Journal of Alloys and Compounds*. 2019;803:364–370. https://doi.org/10.1016/j.jallcom.2019.06.246
7. Astafurova E.G., Panchenko M.Yu., Moskvina V.A., Maier G.G., Astafurov S.V., Melnikov E.V., Fortuna A.S., Reunova K.A., Rubtsov V.E., Kolubaev E.A. Microstructure and grain growth inhomogeneity in austenitic steel produced by wire-feed electron beam melting: the effect of post-building solid-solution treatment. *Journal of Materials Science*. 2020;55:9211–9224. https://doi.org/10.1007/s10853-020-04424-w

**8.** Zuev L.B., Barannikova S.A., Danilov V.I., Gorbatenko V.V. Plasticity: from crystal lattice to macroscopic phenomena. *Progress in Physics of Metals*. 2021;22(1):3–57. https://doi.org/10.15407/ufm.22.01.003

**9.** Zuev L.B., Khon Yu.A., Gorbatenko V.V. Physics of Inhomogeneous Plastic Flow. Moscow: Fizmatlit; 2024:320. (In Russ.).

Зуев Л.Б., Хон Ю.А., Горбатенко В.В. Физика неоднородного пластического течения. Москва: Физматлит; 2024:320.

**10.** Sutton M.A., Orteu J.-J., Schreier H.W. Image Correlation for Shape, Motion and Deformation Measurements. Basic Concepts, Theory and Applications. Berlin: Springer; 2009:317. https://doi.org/10.1007/978-0-387-78747-3

**11.** Zuev L.B., Gorbatenko V.V., Pavlichev K.V. Elaboration of speckle photography techniques for plastic flow analyses. *Measurement Science and Technology*. 2010; 21(5):054014. https://doi.org/10.1088/0957-0233/21/5/054014

**12.** Margerit P., Weisz-Patrault D., Ravi-Chandar K., Constantinescu A. Tensile and ductile fracture properties of as-printed 316L stainless steel thin walls obtained by directed energy deposition. *Additive Manufacturing*. 2021;37:101664. https://doi.org/10.1016/j.addma.2020.101664

**13.** Liu B.X., Yin F.X., Dai X.L., He J.N., Fang W., Chen C.X., Dong Y.C. The tensile behaviors and fracture characteristics of stainless steel clad plates with different interfacial status. *Materials Science and Engineering: A*. 2017;679:172–182. https://doi.org/10.1016/j.msea.2016.10.033

**14.** Boyce B.L., Reu P.L., Robino C.V. The constitutive behavior of laser welds in 304L stainless steel determined by digital image correlation. *Metallurgical and Materials Transactions A*. 2006;37:2481–2492. https://doi.org/10.1007/BF02586221

**15.** Gorbatenko V.V., Danilov V.I., Zuev L.B. Plastic flow instability: Chernov–Lüders bands and the Portevin–Le Chatelier effect. *Technical Physics* 2017;87(3):372-377. (In Russ.). https://doi.org/10.21883/JTF.2017.03.44241.1818

Горбатенко В.В., Данилов В.И., Зуев Л.Б. Неустойчивость пластического течения: полосы Чернова–Людерса и эффект Портевена–Ле Шателье. *Журнал технической физики*. 2017;87(3):372–377. https://doi.org/10.21883/JTF.2017.03.44241.1818

**16.** Danilov V.I., Orlova D.V., Gorbatenko V.V., Danilova L.V. Effect of temperature on the kinetics of localized plasticity autowaves in Lüders deformation. *Metals*. 2023;13(4):773. https://doi.org/10.3390/met13040773

**17.** Danilov V.I., Zuev L.B., Gorbatenko V.V., Orlova D.V., Danilova L.V. Autowave description of the Lüders and Portevin–Le Chatelier phenomena. *Russian Physics Journal*. 2022;65(8): 1411–1418. https://doi.org/10.1007/s11182-023-02784-9

**18.** Danilov V.I., Gorbatenko V.V., Danilova L.V. Kinetics of Lüders deformation as an autowave process. *Izvestiya. Ferrous Metallurgy*. 2022;65(4):261–267. (In Russ.). https://doi.org/10.17073/0368-0797-2022-4-261-267

Данилов В.И., Горбатенко В.В., Данилова Л.В. Кинетика деформации Людерса как автоволнового процесса. *Известия вузов. Черная металлургия*. 2022;65(4):261–267. https://doi.org/10.17073/0368-0797-2022-4-261-267

**19.** Danilov V.I., Orlova D.V., Gorbatenko V.V., Danilova L.V. Lüders and Portevin–Le Chatelier processes in austenitic-martensitic TRIP steel. *Izvestiya. Ferrous Metallurgy*. 2023;66(6):673–680. https://doi.org/10.17073/0368-0797-2023-6-673-680

Данилов В.И., Орлова Д.В., Горбатенко В.В., Данилова Л.В. Процессы Людерса и Портевена–Ле Шателье в аустенитно-мартенситной TRIP-стали. *Известия вузов. Черная Металлургия*. 2023;66(6):673–680. https://doi.org/10.17073/0368-0797-2023-6-673-680

**20.** Barannikova S.A., Li Yu.V. Development kinetics of the plastic wave front at the metal interface. *Izvestiya vuzov. Fizika*. 2020;63(5):19–24. (In Russ.). https://doi.org/10.17223/00213411/63/5/19

Баранникова С.А., Ли Ю.В. Кинетика развития фронтов пластического течения на границе раздела металлов. *Известия вузов. Физика*. 2020;63(5):19–24. https://doi.org/10.17223/00213411/63/5/19

## Information about the Authors

***Dina V. Orlova,*** *Cand. Sci. (Phys.-Math.), Research Associate of the Laboratory of Strength Physics,* Institute of Strength Physics and Materials Science, Siberian Branch of the Russian Academy of Sciences
***ORCID:*** 0000-0003-0068-2542
***E-mail:*** dvo@ispms.ru

***Galina V. Shlyakhova,*** *Cand. Sci. (Eng.), Research Associate of the Laboratory of Strength Physics,* Institute of Strength Physics and Materials Science, Siberian Branch of the Russian Academy of Sciences
***ORCID:*** 0000-0001-9578-2989
***E-mail:*** shgv@ispms.ru

***Mikhail V. Nadezhkin,*** *Cand. Sci. (Eng.), Research Associate of the Laboratory of Strength Physics,* Institute of Strength Physics and Materials Science, Siberian Branch of the Russian Academy of Sciences
***ORCID:*** 0000-0002-4819-7653
***E-mail:*** mvn@ispms.ru

## Сведения об авторах

***Дина Владимировна Орлова,*** *к.ф.-м.н., научный сотрудник лаборатории физики прочности,* Институт физики прочности и материаловедения Сибирского отделения РАН
***ORCID:*** 0000-0003-0068-2542
***E-mail:*** dvo@ispms.ru

***Галина Витальевна Шляхова,*** *к.т.н., научный сотрудник лаборатории физики прочности,* Институт физики прочности и материаловедения Сибирского отделения РАН
***ORCID:*** 0000-0001-9578-2989
***E-mail:*** shgv@ispms.ru

***Михаил Владимирович Надежкин,*** *к.т.н., научный сотрудник лаборатории физики прочности,* Институт физики прочности и материаловедения Сибирского отделения РАН
***ORCID:*** 0000-0002-4819-7653
***E-mail:*** mvn@ispms.ru

## Contribution of the Authors / Вклад авторов

***D. V. Orlova*** – analysis and discussion of experimental results, writing the article final version.
***G. V. Shlyakhova*** – carrying out metallographic studies, describing composite structures.
***M. V. Nadezhkin*** – conducting experiments using the DIC method.

***Д. В. Орлова*** – анализ и обсуждение экспериментальных результатов, написание окончательного варианта рукописи.
***Г. В. Шляхова*** – проведение металлографических исследований, описание структур биметалла.
***М. В. Надежкин*** – проведение экспериментов методом корреляции цифровых изображений.

Received 09.12.2024
Revised 25.12.2024
Accepted 17.01.2025

Поступила в редакцию 09.12.2024
После доработки 25.12.2024
Принята к публикации 17.01.2025